FAA Joint Advanced Materials and Structures

Sixth Annual Technical Review Meeting

May 19-20, 2010

Seattle, Washington

FAILURE OF NOTCHED LAMINATES UNDER OUT-OF-PLANE BENDING

by

J. P. Parmigiani and T. C. Kennedy

School of Mechanical, Industrial, and Manufacturing Engineering

Oregon State University

Corvallis, Oregon 97331

ABSTRACT

The capability of a progressive damage model to predict failure was evaluated for notched laminates under out-of-plane bending using the commercial finite element package ABAQUS and experiments. Laminates studied consisted of 20-ply and 40-ply thickesses with 25.4-mm and 101.6-mm ovaloid center notches. The 40-ply thick laminates exhibited compression-side buckling during testing, requiring the inclusion of delamination interfaces in the finite element model. With the inclusion of interfaces, located near the compression surface and zero-degree plies, agreement with experiment was good, typically within 10%.

1. INTRODUCTION

Damage tolerance requirements have a major influence on the design of aircraft structures made of composite materials. Numerous studies have been devoted to the problem of predicting failure in notched laminates[1]. These investigations have generally focused on the response of laminates to in-plane tension, compression or shear. However, out-of-plane bending, twisting, or shear is a reasonably common load situation in aircraft structures. For example, in an aircraft fuselage, the skin will experience this type of load in the vicinity of stiffening members such as frames and stringers. Very little research has been devoted to this topic[2-5]. As a result, the response of notched laminates subjected to out-of plane loads is not well understood. This uncertainty could lead to unnecessarily conservative design.

There is a need for analysis techniques that are useful for the design of composite aircraft structures under out-of-plane bending. The development of these techniques is complicated by several factors. For example, the laminate does not experience a uniform strain through its thickness as is the case for in-plane loading. This will likely result in a progressive damage development up to final failure that is quite different from the in-plane loading case. Models capable of simulating this behavior will likely require an unusual degree of sophistication. Also, the development of analysis techniques will require significant experimental support to guide the development of the theoretical models. Unfortunately, there

is very little experimental data currently available for the out-of-plane bending case.

The objective of this research was to evaluate the capability of a progressive damage model to predict failure in notched laminates under out-of-plane bending. We have focused on some very basic experiments and modeling efforts involving simple structures (center-notched, unstiffened laminates) under pure bending. The experimental work involved testing of notched laminates under four-point bending. Three laminate types were studied: one with 10% zero-degree plies, one with 30% zero-degree plies, and one with 50% zero-degree plies. The modeling work used the progressive damage model for composites in the ABAQUS finite element program[6] to simulate damage development up to ultimate failure for each laminate tested in four-point bending. This has provided a test of the validity of this model for a loading condition that has not been considered previously[7]. Results for each of these tasks are described below.

2. EXPERIMENTS

Bending experiments were performed on center-notched, unstiffened laminates consisting of three laminate types (10% zero-degree plies, 30% zero-degree plies, and 50% zero-degree plies), two laminate thicknesses (20 plies and 40 plies), and two notch lengths (25.4-mm and 101.6-mm). The notches are in the

shape of ovaloid slits with end radius of 3.175-mm as shown in Figure 1. The 6.35-mm gap between the surfaces of the notch prevented any contact between the notch surfaces on the compression side of the laminate. There are twelve different specimen types depending on the laminate type, laminate thickness, and notch length. Three replicates of each specimen were fabricated with a specimen width to notch-length ratio of five. The laminates were subjected to four-point bending as shown in Figure 2. Several test fixtures were fabricated similar to the one shown in Figure 2. The need for different fixtures was the result of several factors. These include the need to accommodate very large displacements (>150-mm) for some laminates and large loads (>45,000-N) for others. The fixtures were similar in that they applied load to the laminates through 25.4-mm diameter aluminum bars.

3. MODELING

Progressive Damage Model

Our primary objective was to successfully predict the failure load of a notched laminate under out-of-plane bending. This required simulation of the propagation of a notch in the laminate. Williams[8] calculated the crack tip stress and displacement fields for a crack in an infinite isotropic plate under bending using

classical plate theory. He found the usual square root singularity in stress at the crack tip that can be expressed as

$$\sigma = \frac{k_1}{\sqrt{2r}} \frac{2z}{h} \tag{1}$$

where k_1 is the stress intensity factor. A number of studies[9-17] have been conducted to calculate stress intensity factors for orthotropic materials under bending.

In a composite material, a zone of damage of considerable influence is known to develop in advance of the notch. This is the result of a combination of failure modes including fiber breaking, matrix cracking, etc. Consequently, the usual fracture mechanics procedures that have worked successfully in metal structures do not work well for composites[18-20]. The simulation of damage progression in a composite is best done with theories that incorporate principles from the field of damage mechanics. Several such theories[21-25], that treat damage development in the laminate as a whole rather than on a ply-by-ply basis, have been successful in simulating notch growth under in-plane loading. In the case of bending, there is a non-uniform strain through the thickness of the laminate. A theory that treats damage progression at the ply level will be needed for this case.

For our progressive damage analysis, we used the model in ABAQUS for composite materials[26]. This model is based on the work of Matzenmiller, Lubliner, and Taylor[27], Hashin and Rotem[28], Hashin[29], and Camanho and Davila[30]. It considers four different modes of failure: fiber rupture in tension; fiber buckling and kinking in compression; matrix cracking under transverse tension and shearing; and matrix crushing under transverse compression and shearing. It uses concepts from the field of continuum damage mechanics. When damage occurs (microcracking, etc), the effective load carrying area of the material is considered to be reduced, and the concept of an effective stress is introduced to account for the area reduction.

$$\hat{\sigma} = \frac{\sigma}{1 - d} \tag{2}$$

The quantity d is a damage variable that ranges from 0 (no damage) to 1 (development of a macrocrack). From this an effective stress tensor is introduced as

$$\{\hat{\sigma}\} = [M]\{\sigma\} \tag{3}$$

where {σ} is the usual two-dimensional stress in column-matrix form in principal material directions, and M is a damage operator given as

$$[M] = \begin{bmatrix} \frac{1}{1-d_f} & 0 & 0 \\ 0 & \frac{1}{1-d_m} & \\ & & \frac{1}{1-d_s} \end{bmatrix} \quad (4)$$

where d_f, d_m, and d_s are damage variables characterizing fiber, matrix, and shear damage.

The constitutive relation for the material is affected by damage and results in a strain-softening response given by

$$\{\sigma\} = [C_d]\{\varepsilon\} \quad (5)$$

where $\{\varepsilon\}$ is the usual two-dimensional strain in column matrix form and $[C_d]$ is the effective elasticity matrix given by

$$[C_d] = \frac{1}{D}\begin{bmatrix} (1-d_f)E_1 & (1-d_f)(1-d_m)\nu_{21}E_1 & 0 \\ (1-d_f)(1-d_m)\nu_{12}E_2 & (1-d_f)E_2 & 0 \\ 0 & 0 & (1-d_s)G_{12} \end{bmatrix} \quad (6)$$

where $D=1-(1-d_f)(1-d_m)\nu_{12}\,\nu_{21}$, and E_1, E_2, G_{12}, ν_{12} and ν_{21} are the usual orthotropic elastic constants.

The initiation of damage depends on which of the four modes of failure, described earlier, is activated. The criteria for initiation uses Hashin's theory and is governed by the following relations:

Fiber tension ($\hat{\sigma}_{11} \geq 0$): $$\left(\frac{\hat{\sigma}_{11}}{X^T}\right)^2 + \alpha\left(\frac{\hat{\tau}_{12}}{S^L}\right)^2 = 1 \quad (7)$$

Fiber compression ($\hat{\sigma}_{11} < 0$): $$\left(\frac{\hat{\sigma}_{11}}{X^C}\right)^2 = 1 \quad (8)$$

Matrix tension ($\hat{\sigma}_{22} \geq 0$): $$\left(\frac{\hat{\sigma}_{22}}{Y^T}\right)^2 + \left(\frac{\hat{\tau}_{12}}{S^L}\right)^2 = 1 \quad (9)$$

Matrix compression ($\hat{\sigma}_{22} < 0$): $$\left(\frac{\hat{\sigma}_{22}}{2S^T}\right)^2 + \left[\left(\frac{Y^C}{2S^T}\right)^2 - 1\right]\frac{\hat{\sigma}_{22}}{Y^C} + \left(\frac{\hat{\tau}_{12}}{S^L}\right)^2 = 1 \quad (10)$$

where X^T is the tensile strength in the fiber direction, X^C is the compressive strength in the fiber direction, Y^T is the tensile strength in the direction perpendicular to the fibers, Y^C is the compressive strength in the direction perpendicular to the fibers, S^L is the longitudinal shear strength, S^T is the transverse shear strength, and α is a coefficient that determines the contribution of the shear stress to the fiber tensile initiation criterion.

The incorporation of strain softening into a finite element analysis usually results in calculations that are mesh sensitive. This occurs because as the mesh is refined, there is a tendency for the damage zone to localize to a zero volume. This leads to prediction of structural failure with zero energy dissipation, which is physically impossible. Several techniques have been proposed to address this issue. One of the simplest, which was pioneered by Hillerborg[31], is to use a stress-displacement law rather than a stress-strain law in the damaged material. The ABAQUS program accomplishes this by introducing a characteristic length L_c based on element size. From this, equivalent displacements and equivalent stresses are defined for the four modes of failure as follows:

Fiber tension ($\hat{\sigma}_{11} \geq 0$):

$$\delta_{eq}^{ft} = L^c \sqrt{\langle \varepsilon_{11} \rangle^2 + \alpha \varepsilon_{12}^2} \tag{11}$$

$$\sigma_{eq}^{ft} = \frac{\langle \sigma_{11} \rangle \langle \varepsilon_{11} \rangle + \alpha \tau_{12} \varepsilon_{12}}{\delta_{eq}^{ft} / L^c} \tag{12}$$

Fiber compression ($\hat{\sigma}_{11} < 0$):

$$\delta_{eq}^{fc} = L^c \langle -\varepsilon_{11} \rangle \tag{13}$$

$$\sigma_{eq}^{fc} = \langle -\sigma_{11} \rangle \tag{14}$$

Matrix tension ($\hat{\sigma}_{22} \geq 0$):

$$\delta_{eq}^{mt} = L^c \sqrt{\langle \varepsilon_{22} \rangle^2 + \varepsilon_{12}^2} \tag{15}$$

$$\sigma_{eq}^{mt} = \frac{\langle \sigma_{22} \rangle \langle \varepsilon_{22} \rangle + \tau_{12}\varepsilon_{12}}{\delta_{eq}^{mt} / L^c} \tag{16}$$

Matrix compression ($\hat{\sigma}_{22} < 0$):

$$\delta_{eq}^{mc} = L^c \sqrt{\langle -\varepsilon_{22} \rangle^2 + \varepsilon_{12}^2} \tag{17}$$

$$\sigma_{eq}^{mc} = \frac{\langle -\sigma_{22} \rangle \langle -\varepsilon_{22} \rangle + \tau_{12}\varepsilon_{12}}{\delta_{eq}^{mc} / L^c} \tag{18}$$

For a given failure mode the stress-displacement law takes on the form shown in Figure 5. The part of the curve with a positive slope (OA) follows the usual linear elastic relationship and can be expressed as

$$\sigma_{eq} = \frac{\delta_{eq}}{\delta_{eq}^0}\sigma_{eq}^0 \tag{19}$$

The apex of the cure (A) represents the initiation of damage. Displacement beyond this point results in a decreasing stress. This part of the curve can be represented by

$$\sigma_{eq} = \frac{(\delta_{eq}^f - \delta_{eq})}{(\delta_{eq}^f - \delta_{eq}^0)}\sigma_{eq}^0 \tag{20}$$

After experiencing damage, the material unloads and reloads along line OB which has a smaller slope than the original line OA. This reduced slope is accounted for using the damage variable d as

$$slopeOB = \frac{\sigma_{eq}^{0}}{\delta_{eq}^{0}}(1-d) \tag{21}$$

Combining the last three equations with eq. (2) gives the damage variable as

$$d = \frac{(\delta_{eq} - \delta_{eq}^{0})\delta_{eq}^{f}}{(\delta_{eq}^{f} - \delta_{eq}^{0})\delta_{eq}} \tag{22}$$

When running an analysis model in ABAQUS, the following parameters must be specified: X^T, X^C, Y^T, Y^C, S^L, S^T, α, and the dissipation energies (area under OAC) for each failure mode: G_{ft}, G_{fc}, G_{mt}, and G_{mc}.

Delamination Modeling

We also need to allow for delamination between plies. This effect was modeled using the Virtual Crack Closure Technique (VVCT)[32]. This technique uses the principles of linear elastic fracture mechanics and allows crack propagation when a critical value of the strain energy release rate is attained. The crack must

propagate along a predefined path at the interface between elements. The strain energy release rate is calculated from the energy required to close the crack over one element length. Crack growth is assumed to occur when the following criterion is met

$$\frac{G_I}{G_{Ic}} + \frac{G_{II}}{G_{IIc}} + \frac{G_{III}}{G_{IIIc}} \geq 1 \tag{23}$$

where G_j is the strain energy release rate for mode j (j=I,II,III), and G_{jc} is the critical strain energy release rate for mode j. The critical strain energy release rate must be determined from interlaminar fracture experiments.

Finite Element Models

Two types of finite element models were constructed - one that allowed delamination between plies and another that did not. The type which allowed delamination was composed of eight-node continuum shell elements stacked through the thickness of the laminate as shown in Figure 4 for a 25.4-mm long notch. Only one half of the plate is modeled (although this symmetry assumption is not strictly valid because of some weak coupling between bending and twisting, it had negligible effect on the failure load). The interior interfaces between the element layers were allowed to debond according to the VCCT model. Various locations of the interfaces were explored to determine their effect on failure load, as will be described in the next section. The second type of

model, which did not allow Delamination (i.e. no interfaces), was composed of a single layer of four-node conventional shell elements. Both types of models were also constructed for laminates with a 25.4-mm and a 101.6-mm long notch.

4. EXPERIMENTAL RESULTS AND DAMAGE ANALYSIS

The maximum moment that could be carried by the laminate (i.e., the failure load) was measured in the experiments and calculated using the finite element computer models. During the experiments the 20-ply thick laminates exhibited negligible visible damage before failure, which was sudden and usually resulted in the laminate being broken into two pieces as shown in Figure 5. The 40-ply thick laminates exhibited a gradual progression of damage, which usually began with wrinkling of the outer ply on the compression side. Generally, this was followed by delamination at the outermost zero-degree ply and fracture of the plies between the outermost zero-degree ply and the surface. There was also some delamination between the second outermost zero-degree ply and the surface. The tension side of the laminate generally exhibited considerably less visible damage. This is illustrated in Figure 6 which shows a close-up view of the edge of the laminate (the light colored plies are the zero-degree plies). In some cases it was observed that the plies between the outermost zero-degree ply and the surface buckled before fracturing as shown in Figure 7a. This phenomenon was captured by the model as shown in Figure 7b.

The first calculations were performed using the models with no delamination interfaces, as described in the previous section. For the 20-ply thick laminate, model results, for the six cases examined, varied from experiment from 11.5% lower to 9.5% higher with an average difference of 2.9% lower. For the 40-ply thick laminate, model results, for the six cases examined, varied from experiment from 0.1% lower to 28.4% higher with an average difference of 16.9% higher. These results are shown in Figures 8 – 11.

As described above, experiments showed that the thicker, 40-ply, laminates experienced delamination during fracture, allowing plies between the delamination and the surface to buckle outward. This causes a redistribution of the stress that leads to further delamination and fracturing of additional plies. Because the progressive damage models used considered the plies to be perfectly bonded (i.e. no delamination interfaces existed in the model), this buckling failure mechanism was not replicated in the FEA results.

In order to more accurately model the laminate fracture, two delamination interfaces were added to the 40-ply models. Two interfaces were also added to the 20-ply laminates to determine their effect. Interfaces were placed below (away from the compression surface) the outer-most compression-side zer-degree ply and below the second outer-most zero-degree ply. As described

previously, these locations corresponded to where delamination was observed in the experiments.

As expected, based on the observed failure modes from the experiments, the addition of these interfaces to the models had a small effect on the calculated failure loads for the 20-ply laminates and a much greater effect for the 40-ply laminates. For the 20-ply laminate, model results, for the six cases examined, now varied from experiment from 5.3% lower to 9.1% higher with an average difference of 1.7% lower as compared to 2.9% lower with no interfaces. For the 40-ply thick laminate, model results now varied from experiment from 18.1% lower to 3.0% higher with an average difference of 6.7% lower as compared to 16.9% lower with no interfaces. These results are also shown in figures 8 – 11.

In order to better understand the effect of delamination on the model, additional interfaces were added. In addition to interfaces below the outer-most and second outer-most zero-degree plies, interfaces were placed below the outer-most ply and above the outer-most zero-degree ply for a total of four interfaces. A necessary exception was the 20-ply, 10% zero-degree-ply laminate. Here only one zero-degree ply existed on the compression side, so only three interfaces were created. Additionally, due to the excessively long run times associated with the 101.6-mm notch laminates, only 25.4-mm laminates were included in this aspect of the study.

In general, the additional delamination interfaces had a negligible effect on the calculated fracture loads. For the 20-ply laminates, with 25.4-mm notches, the difference between experimentally measured and model-predicted failure load varied from an average of 1.5% (model higher) with no interfaces to 2.4% (model higher) with two interfaces to -2.4% (model lower) with four (or three as described above) interfaces. For the 40-ply laminates, with 25.4-mm notches, the results were an average of 23.5% (model higher) with no interfaces, 1.7% (model higher) with two interfaces and 6.4% (model higher) with four interfaces. These results are also shown in figures 8 – 11 and are summarized in Table 1.

5. CONCLUSION

The objective of this research was to evaluate the capability of a progressive damage model to predict failure in notched laminates under out-of-plane bending. To this end, the failure moment was measured, via experiment, and calculated, via finite element analysis, for ovaloid center-notched plates of twelve different laminate lay-ups. These layups consisted of 10%, 30%, and 50% zero-degree plies in 20 and 40 ply thick plates with 25.4-mm and 101.6-mm long ovaloids. Experimentally, failure of the 20-ply laminates occurred with little visible damage. Failure of the 40-ply laminates occurred with considerable ply compression-driven delamination and buckling near the plate surface and near zero-degree plies. Finite element models, using the Hashin damage criteria and no delamination interfaces, showed good agreement with experiment (typically

within 10%) for all 20-ply laminates. Lack of delamination interfaces in the 40-ply finite element models resulted in significant discrepancies with experiment, with differences up to nearly 30%.

The addition of two interfaces to the models, placed corresponding to where delamination occurred in the 40-ply experimental specimens, had no adverse effect on either the 25.4-mm or 101.6-mm notch 20-ply laminate model results, but did greatly improve the accuracy of the 25.4-mm notch 40-ply models. For the 101.6-mm notch 40 ply models, including two interfaces did significantly change the predicted failure load, but resulted in uncharacteristically large differences with experiment. Increasing the number of interfaces from two to four did not significantly change the results for either the 20 ply or 40 ply 25.4-mm notched laminates.

In general, this research indicates that failure of notched laminates can be successfully predicted with progressive damage models if interfaces are included where delamination is likely to occur. Given that it may not be know where delamination will occur, it is also noted that there does not appear to be an accuracy penalty for including interfaces when delamination does not occur.

REFERENCES

1. J. Awerbuch and M.S. Madhukar, "Notched strength of composite laminates: predictions and experiments - a review," Journal of Reinforced Plastics and Composites, 4 (1985): 1-149.

2. D.L. Jones and N. Subramonian, “An analytical and experimental study of the plate tearing mode of fracture,” Engineering Fracture Mechanics, 17 (1983): 47-62.

3. M.J. Shuart and C.B. Prasad, ”Analysis and experiments for composite laminates with holes and subjected to 4-point bending, AIAA/ASME/ASCE/AHS Structures, Structural Dynamics & Materials Conference (1990): 748-758.

4. R.D. Bradshaw and S.S. Pang, “Failure analysis of composite laminated plates with circular holes under bending”, American society of Mechanical Engineers, Petroleum Division (Publication) PD, V 37, Composite Material Technology (1991): 125-135.

5. C.B. Prasad, M.J. Shuart, N.J. Bains, and M. Rouse,”Effects of cutouts on the behavior of symmetric composite laminates subjected to bending and twisting loads,” NASA Report N95-28844.

6. I. Lapczyk and J.A. Hurtado, “Progressive damage modeling in fiber-reinforced materials,” Composites: Part A, 38 (2007): 2333-2341.

7. P. Maimi, P.P. Camanho, J.A. Mayugo, and C.G. Davila, “A thermodynamically consistent damage model for advanced composites”, *NASA/TM-2006-214282* (2006)

8. M. Williams, “ The bending stress distribution at the base of a stationary crack, Journal of Applied Mechanics, 28 (1961): 78-82.

9. N. Wang, “Effects of plate thickness on the bending of an elastic plate containing a crack”, Journal of Mathematics and Physics, 47, (1968): 371-390.

10. F. Delale and F. Erdogan, “The effect of transverse shear under skew-symmetric loading,” Journal of Applied Mechanics, 46 (1979): 618-624.

11. R.S. Alwar and K.N. Ramachandran, ”Three-dimensional finite element analysis of cracked thick plates in bending,” International Journal for Numerical Methods in Engineering, 19 (1983): 293-303.

12. B.H. Wu and F. Erdogan, “The surface and through crack problems in orthotropic plates,” International Journal of Solids and Structures 25 (1989): 167-188.

13. M.J. Young and C.T. Sun, “On the strain energy release rate for a cracked plate subjected to out-of-plane bending moment,” International Journal of Fracture, 60 (1993): 227-247.

14. A.T. Zehnder and C.Y. Hui, “Stress intensity factors for plate bending and shearing problems,” ASME Journal of Applied Mechanics, 61 (1994): 719-722.

15. A. Zucchini, C.Y. Hui, and A.T. Zehnder, “Crack tip stress fields for thin, cracked plates in bending, shear, and twisting: a comparison of plate theory and three-dimensional elasticity solutions,” International Journal of Fracture, 104 (2000): 387-407.

16. L. Chattopadhyay, “Analytical solution for an orthotropic plate containing cracks,” International Journal of Fracture,134 (2005): 305-317.

17. A.T. Zehnder and M.J. Viz, “Fracture mechanics of thin plates and shells under combined membrane, bending, and twisting loads,” Applied Mechanics Reviews, 58 (2005): 37-48.

18. T.H. Walker, W.B. Avery, L.B. Ilcewicz, and C.C. Poe, “Tension fracture of laminates for transport fuselage – part 1: material screening,” Second NASA Advanced Technology Conference, NASA CP3154 (1991): 197-238.

19. T.H. Walker, L.B. Ilcewicz, D.R. Polland, and C.C. Poe, “Tension fracture of laminates for transport fuselage – part 2: large notches,” Third NASA Advanced Technology Conference, NASA CP 3178 (1992): 727-758.

20. L.B. Ilcewicz, T.H. Walker, D.P. Murphy, B. Dopker, and D.B. Scholz, “Tension fracture of laminates for transport fuselage – part 4: damage tolerance analysis,” Fourth NASA Advanced Technology Conference, NASA CP 3229, (1993): 264-298.

21. J. Backlund and C.G. Aronsson, “Tensile fracture of laminates with holes,” Journal of Composite Materials, 20 (1986): 259-286.

22. C.G. Aronsson and J. Backlund, “Tensile fracture of laminates with cracks,” Journal of Composite Materials, 20, (1986): 287-307.

23. B. Dopker, D.P. Murphy, L.B. Ilcewicz, T.H. Walker, “Damage Tolerance Analysis of Composite Transport Fuselage Structure,” 35th AIAA/ASME/ASCE/AHS/ASC Structures, Structural Dynamics, and Materials Conference, Hilton Head, South Carolina (1994): 58A-1-58A-8.

24. T.C. Kennedy and M.F. Nahan, “A simple nonlocal damage model for predicting failure of notched laminates,” Composite Structures, 35 (1996): 229-236.

25. T.C. Kennedy and M.F. Nahan, “A simple nonlocal damage model for predicting failure in a composite shell containing a crack,” Composite Structures, 39 (1997): 85-91.

26. ABAQUS Analysis User’s Manual, Version 6.7, Simulia, Providence, Rhode Island (2007).

27. A.J. Matzenmiller, J. Lubliner, and R.L. Taylor, “A Constitutive Model for Anisotropic Damage in Fiber-Composites,” Mechanics of Materials, 20 (1995): 125–152.

28. Z. Hashin, and A. Rotem, “A Fatigue Criterion for Fiber-Reinforced Materials,” Journal of Composite Materials, 7 (1973): 448–464.

29. Z. Hashin, “Failure Criteria for Unidirectional Fiber Composites,” Journal of Applied Mechanics, 47 (1980): 329–334.

30. P.P. Camanho and C.G. Davila, “Mixed-Mode Decohesion Finite Elements for the Simulation of Delamination in Composite Materials,” NASA/TM-2002–211737 (2002): 1–37.

31. A. Hillerborg, M. Modeer, and P.E. Petersson, ”Analysis of crack formation and crack growth in concrete by means of fracture mechanics and finite elements, Cement Concrete Research, 6 (1976): 773-782.

32. R. Krueger, ”Virtual crack closure technique: history, approach, and applications,” Applied Mechanics Reviews, 57 (2004): 109-143.

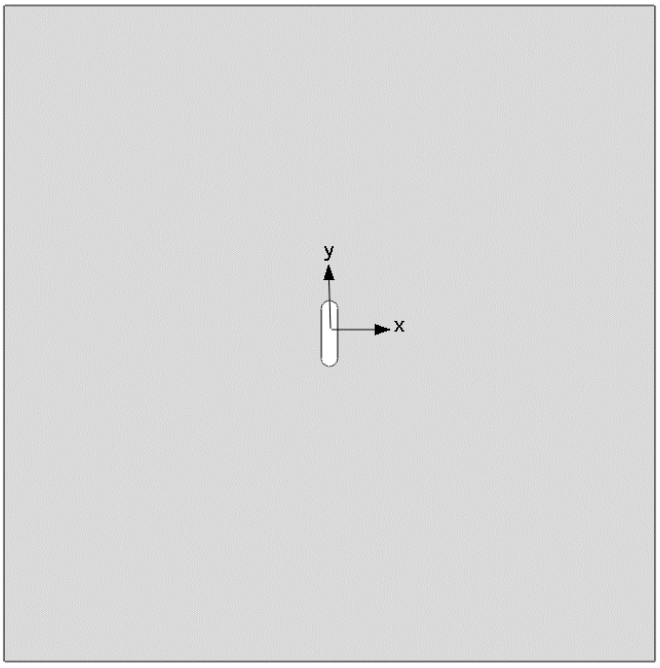

Figure 1 Ovaloid notch in a plate

Figure 2 Four-point bending test fixture

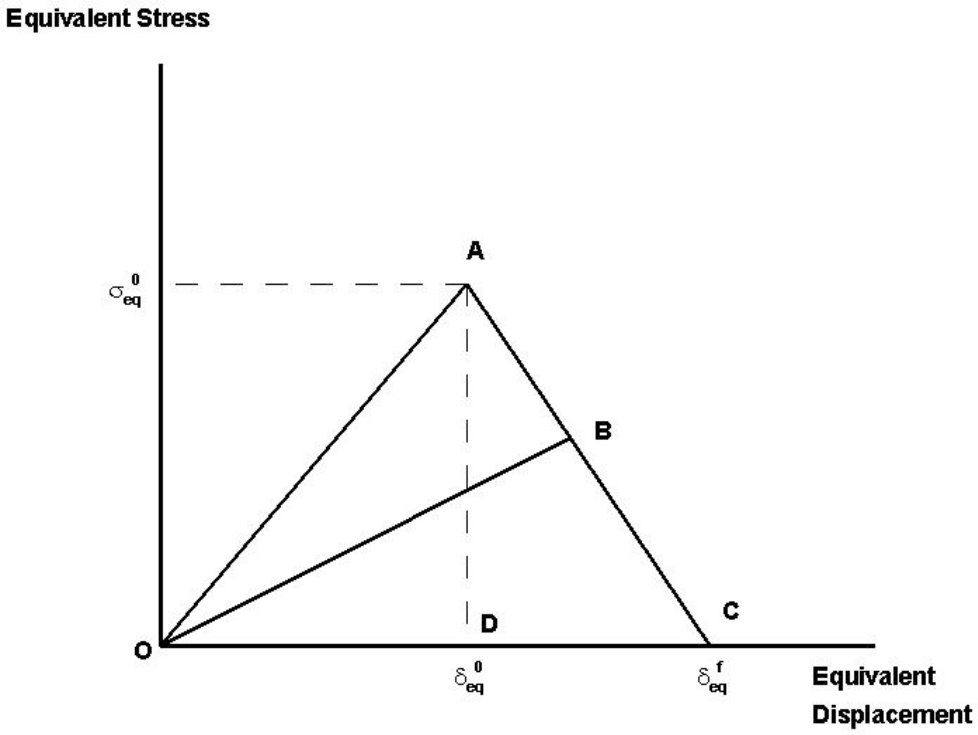

Figure 3 Stress-displacement constitutive law used in ABAQUS

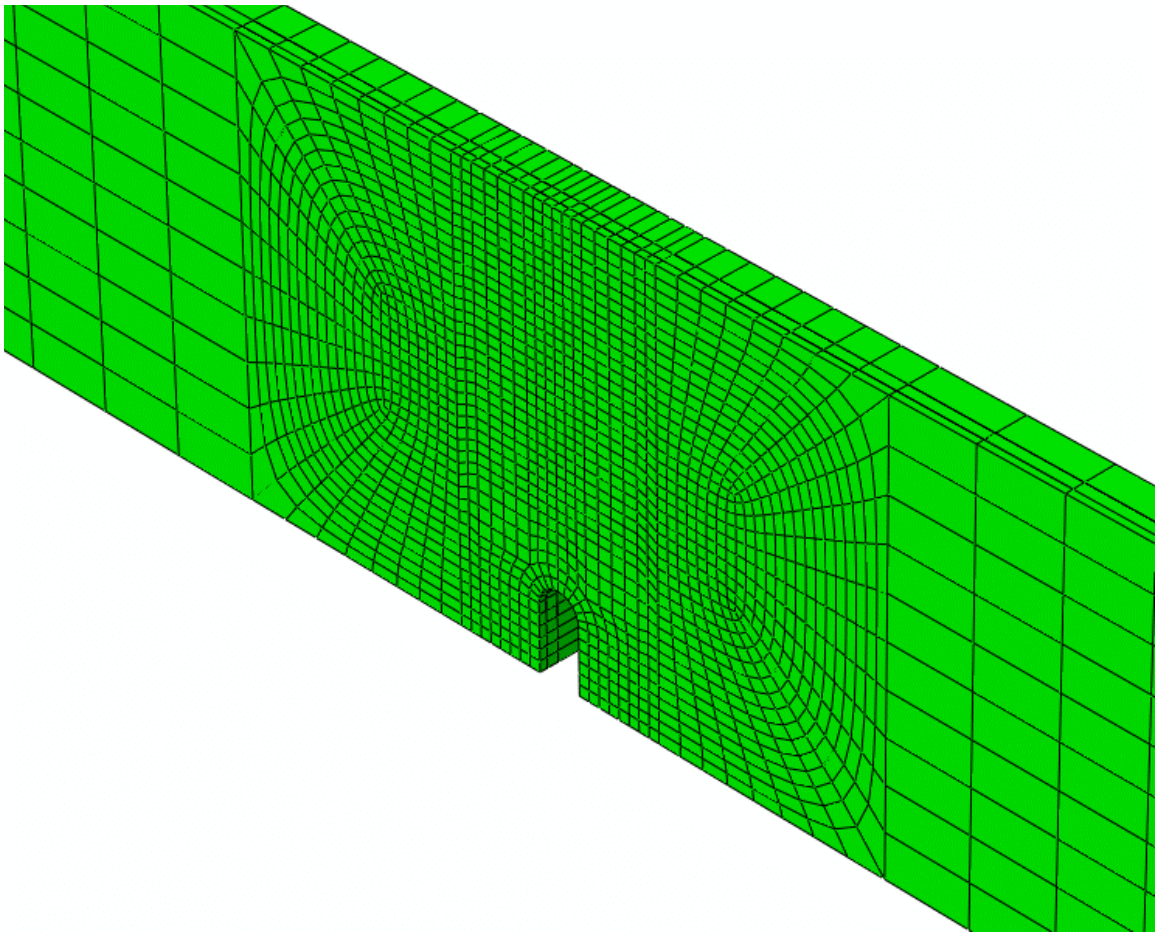

Figure 4 Half-symmetry finite element model with delamination interfaces for laminates with a 1-in notch

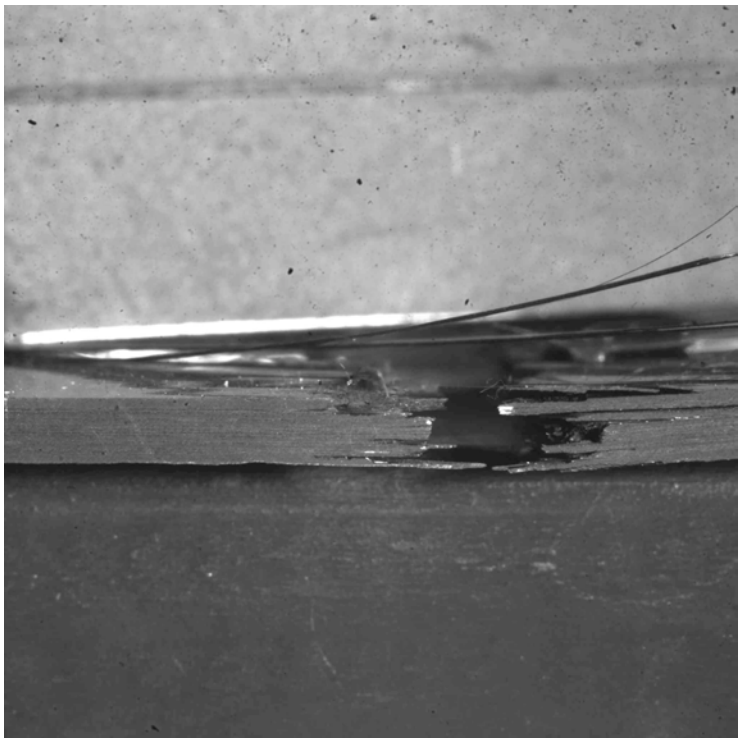

Figure 5 Post-failure photo of a 20-ply thick laminate

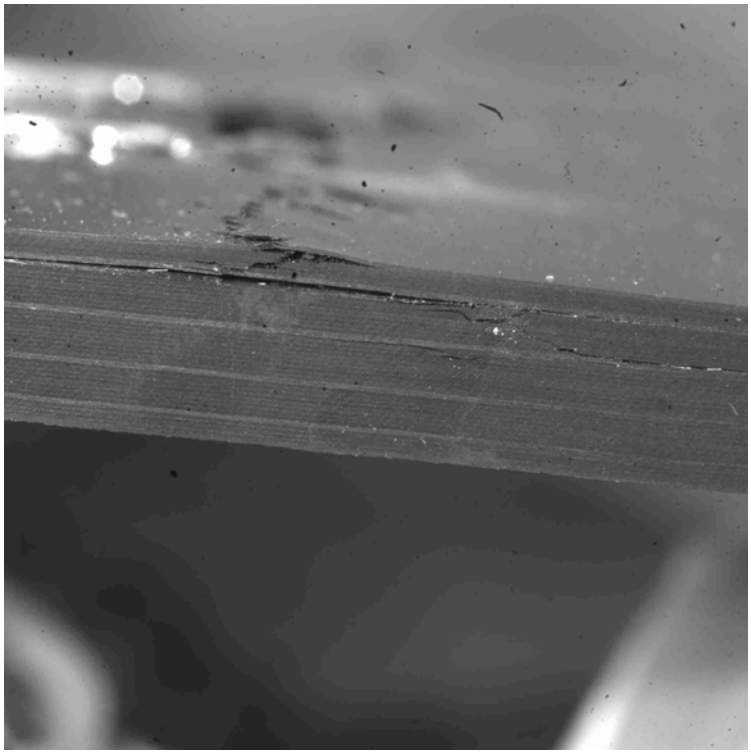

Figure 6 Post-failure photo of a 40-ply thick laminate

b) Experiment

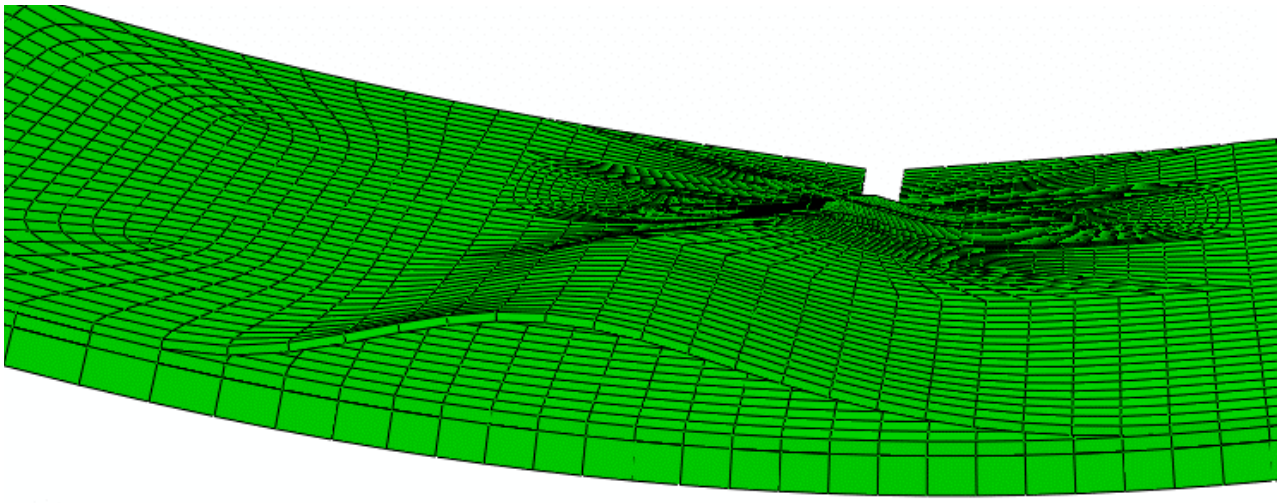

a) Model

Figure 7 Post-delamination buckling

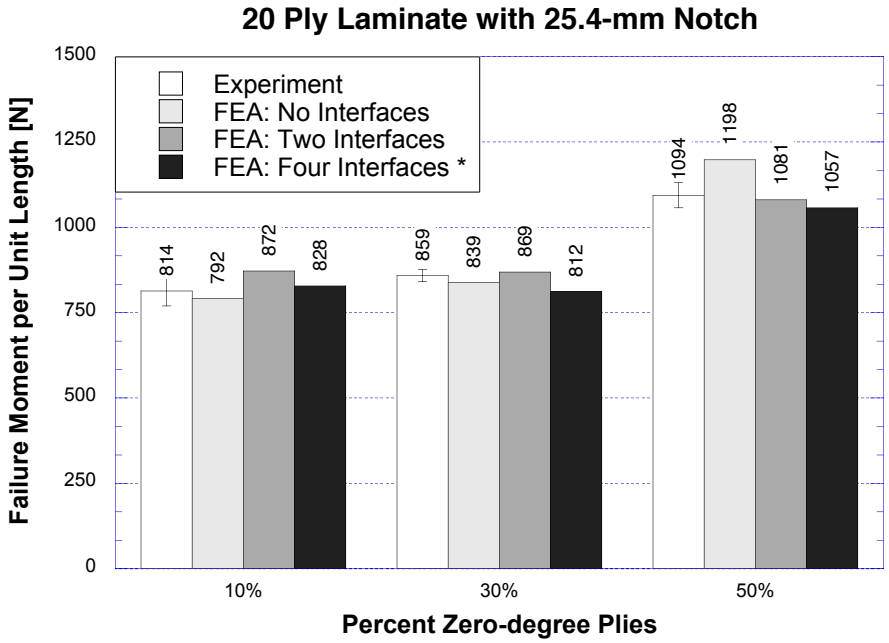

Figure 8 Failure moment for 20-ply laminates with 25.4-mm notch

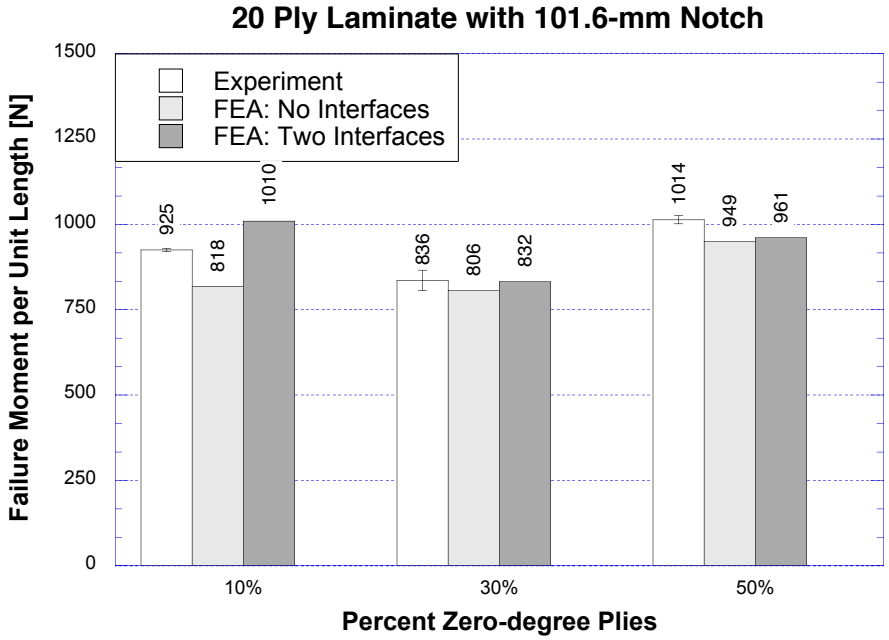

Figure 9 Failure moment for 20-ply laminates with 101.6-mm notch

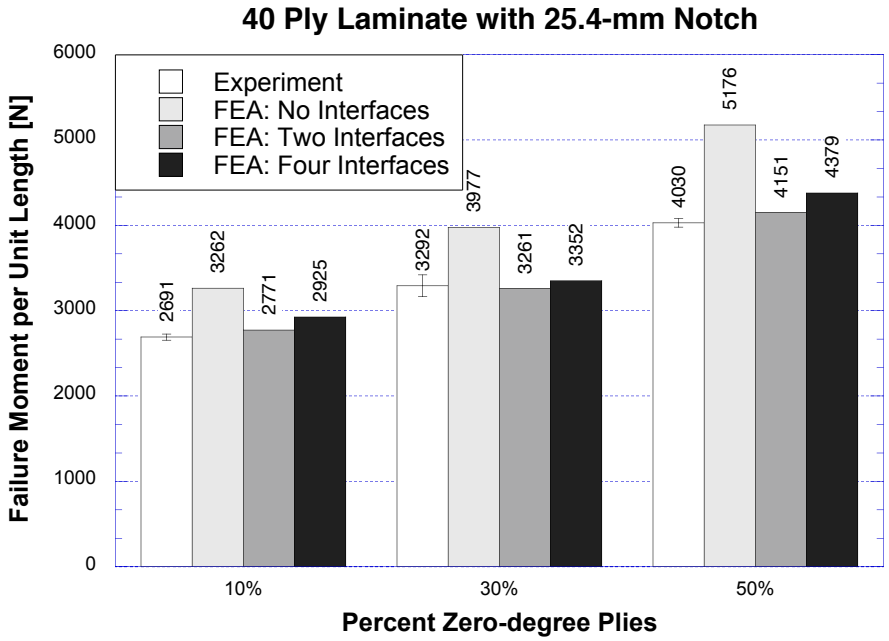

Figure 10 Failure moment for 40-ply laminates with 25.4-mm notch

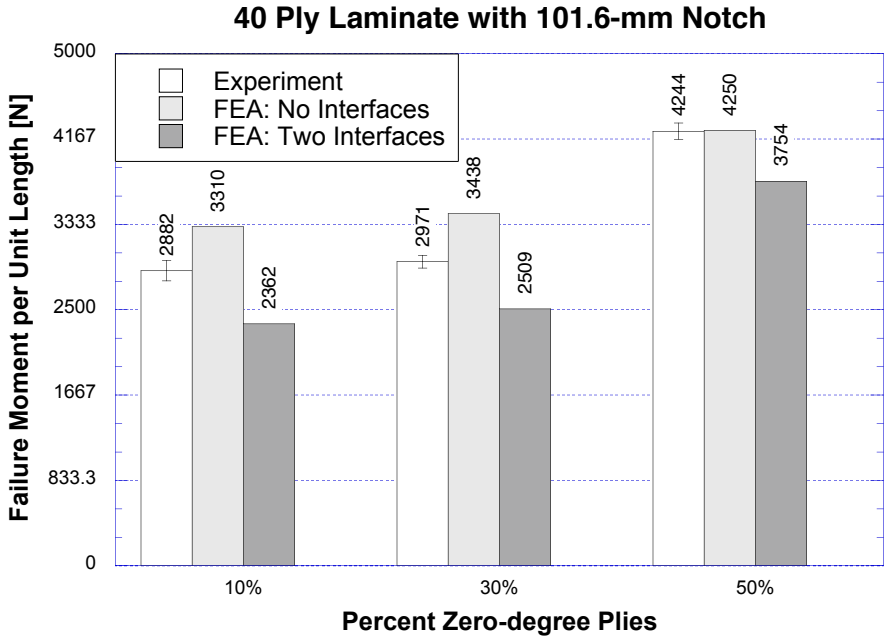

Figure 11 Failure moment for 40-ply laminates with 101.6-mm notch

Table 1 Comparison of finite element model calculations and experimental results for all cases studied.

Number of Plies	Notch Length [mm]	Percent Zero-degree plies	FEA: Percent Difference from Experiment		
			No Interfaces	Two Interfaces	Four Interfaces
20	25.4	10	-2.7%	7.1%	1.7% *
		30	-2.2%	1.3%	-5.4%
		50	9.5%	-1.2%	-3.4%
	101.6	10	-11.5%	9.1%	
		30	-3.7%	-0.5%	
		50	-6.4%	-5.3%	
40	25.4	10	21.2%	3.0%	8.7%
		30	20.8%	-0.9%	1.8%
		50	28.4%	3.0%	8.7%
	101.6	10	14.8%	-18.1%	
		30	15.7%	-15.6%	
		50	0.1%	-11.5%	